

Deterministic Variational Inference for Neural SDEs

Andreas Look¹, Jan Peters², Melih Kandemir¹

¹Bosch Center for Artificial Intelligence
Renningen, Germany
{firstname.lastname}@de.bosch.com

²Intelligent Autonomous Systems
TU Darmstadt, Germany
peters@ias.tu-darmstadt.de

Abstract

Neural Stochastic Differential Equations (NSDEs) model the drift and diffusion functions of a stochastic process as neural networks. While NSDEs are known to predict time series accurately, their uncertainty quantification properties remain unexplored. Currently, there are no approximate inference methods, which allow flexible models and provide at the same time high quality uncertainty estimates at a reasonable computational cost. Existing SDE inference methods either make overly restrictive assumptions, e.g. linearity, or rely on Monte Carlo integration that requires many samples at prediction time for reliable uncertainty quantification. However, many real-world safety critical applications necessitate highly expressive models that can quantify prediction uncertainty at affordable computational cost. We introduce a variational inference scheme that approximates the posterior distribution of a NSDE governing a latent state space by a deterministic chain of operations. We approximate the intractable data fit term of the evidence lower bound by a novel bidimensional moment matching algorithm: vertical along the neural net layers and horizontal along the time direction. Our algorithm achieves uncertainty calibration scores that can be matched by its sampling-based counterparts only at significantly higher computation cost, while providing as accurate forecasts on system dynamics.

1 Introduction

Accompanying time series predictions with calibrated uncertainty scores is a challenging problem. The main difficulty is that uncertainty assessments for individual time points propagate, causing local errors to impair the predictions on the whole sequence. While calibrated prediction is well-studied for feed-forward neural networks [Platt, 1999, Thiagarajan et al., 2020], the same problem is a relatively new challenge for predictors with feedback loops. The few prior work is restricted to post-hoc calibration of deterministic recurrent neural nets [Kuleshov et al., 2018, Cui et al., 2020].

We report the first study on the uncertainty quantification characteristics of *Neural Stochastic Differential Equations* (NSDEs) [Tzen & Raginsky, 2019, Li et al., 2020]. A Neural SDE consists of a drift neural net governing the deterministic component of a vector field and a diffusion neural net governing the instantaneous distortions. Neural SDEs have a large potential to provide an attractive tool to the machine learning community due to their strong theoretical links to *Recurrent Neural Nets* (RNNs), *Neural ODEs* (NODEs), and *Gaussian Processes* (GPs) [Särkkä & Solin, 2019, Hegde et al., 2019]. While multiple studies have observed NSDEs to bring encouraging success in prediction accuracy, none has thus far investigated their performance in uncertainty quantification. Yet, an essential benefit of modeling stochasticity is to account for uncertainty in a reliable way.

Existing approximate inference methods for SDEs either heavily rely on *Monte Carlo* (MC) sampling [Li et al., 2020, Tzen & Raginsky, 2019] or make overly restrictive assumption such as the approximate

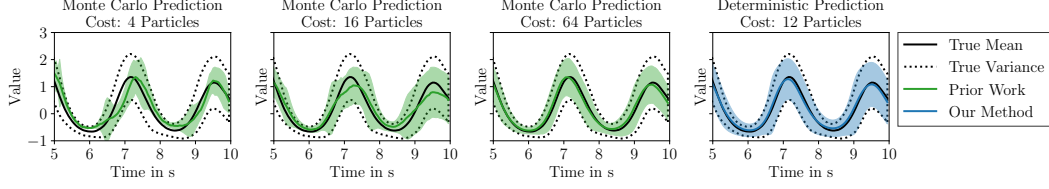


Figure 1: Our deterministic prediction method provides well-calibrated uncertainty scores with a computational cost equal to 12 particles. Reaching a comparable level of calibration by Monte Carlo sampling demands at least 64 particles.

distribution being linear [Archambeau et al., 2007]. We make the central observation that solving NSDEs with MC sampling requires a prohibitively large sample set, i.e. computation time, for accurate uncertainty quantification. As safety critical applications raise the need for both i) flexible models without the linearity restriction, and ii) access to accurate uncertainty quantification at a reasonable computational cost, we propose a novel deterministic *Variational Inference (VI)* algorithm. As our main contribution we approximate the intractable data fit term in the *Evidence Lower Bound (ELBO)* by a computationally affordable deterministic algorithm that approximates intractable expectation and covariance integrals by matching moments horizontally across time and vertically across neural net layers. As the algorithm performs moment matching in two uncoupled directions, we refer to it as *Bidimensional Moment Matching (BMM)*, which is applicable at training and test time. In addition to providing a novel solution to an open problem as a whole, the algorithm contains technical originalities in its intermediate steps, such as employing Steins’s lemma for the first time to simplify the covariance calculation of a state space model, as well as backpropagating through the approximate expectation of the Jacobian of a neural net with respect to random input. As exemplified in Fig. 1, NSDE prediction with MC sampling requires a large sample set to catch up with the calibration level of our deterministic prediction method. We observe in three applications that our method delivers the highest accuracy and most calibrated uncertainties.

2 Neural Stochastic Differential Equations as State Space Models

We study the family of state space models that describes the dynamics of a D_z –dimensional latent stochastic process $z(t)$ as a non-linear time-invariant SDE

$$dz(t) = f_\theta(z(t))dt + L_\phi(z(t))dw(t), \quad \text{Transition model} \quad (1)$$

$$y(t) \sim p(y(t)|z(t)), \quad \text{Observation model} \quad (2)$$

which is observed via a D_y –dimensional variable $y(t)$. The latent dynamics is defined via the drift function $f_\theta(z(t)) : \mathbb{R}^{D_z} \rightarrow \mathbb{R}^{D_z}$, which is governing the deterministic component of the SDE, and the diffusion function $L_\phi(z(t)) : \mathbb{R}^{D_z} \rightarrow \mathbb{R}^{D_z \times D_z}$, which models the stochasticity of the system. We assume that both f_θ and L_ϕ are neural nets with arbitrary architectures that ensure Lipschitz-continuity and linear growth. Further, dt is the time increment and $w(t)$ is a D_z –dimensional standard Wiener process that injects instantaneous noise into the dynamics following a normal distribution with variance proportional to the time increment. In order to make a prediction at a time point t_{n+1} , an initial value $z(t_n)$ at time point t_n needs to be provided and the below system to be solved

$$z(t_{n+1}) = z(t_n) + \int_{t_n}^{t_{n+1}} f_\theta(z(t))dt + \int_{t_n}^{t_{n+1}} L_\phi(z(t))dw(t). \quad (3)$$

The integral involving the drift function is defined as a Lebesgue integral and the second integral involving the diffusion with respect to the Wiener process $dw(t)$ is defined as an Itô integral [Oksendal, 1992]. The randomness induced at every infinitesimal time step by $dw(t)$ makes the solution $z(t_{n+1})$ a random variable that follows a probability distribution $p(z(t_{n+1})|z(t_n))$.

2.1 Variational Inference

Given a time series $Y = \{y(t_1), \dots, y(t_N)\}$ of length N observed at arbitrarily-spaced time points t_1, \dots, t_N , one can express its marginal likelihood with respect to the state space model in Eq. 1 as

$$p(Y) = \int p(Y|Z)p(Z)dZ = \int p(z(t_0)) \prod_{n=1}^N p(z(t_n)|z(t_{n-1}))p(y(t_n)|z(t_n))dZ. \quad (4)$$

We are interested in fitting the model parameters θ and ϕ to an observed sample set $\mathcal{D} = \{Y_1, \dots, Y_M\}$ consisting of M time series of arbitrary lengths and resolutions. This can be achieved by evaluating the above marginal likelihood and maximizing it by gradient-ascent backpropagating through θ and ϕ . As the integral in Eq. 4 is analytically intractable for non-trivial choices of f_θ and L_ϕ , we approximate it by variational inference.

NSDE training involves fitting thousands of free parameters even for modest neural net architectures, making many of the existing techniques in the standard SDE literature [Ryder et al., 2018, Abbati et al., 2019] inapplicable to NSDEs due to computational limitations. Parameter estimation via variational inference for NSDEs has been proposed earlier in Li et al. [2020], Tzen & Raginsky [2019] by defining a prior distribution for the learnable target process and approximating intractable terms by MC sampling. We develop a deterministic alternative that provides high calibration of predictive uncertainty at significantly less computational cost. Inspired by the variational inference practices in sparse GPs [Titsias & Lawrence, 2010], we choose the approximate posterior to be

$$q(Z) = q(z(t_0)) \prod_{n=1}^N p(z(t_n)|z(t_{n-1})), \quad (5)$$

with the recognition model $q(z(t_0))$ and the true transition kernel $p(z(t_n)|z(t_{n-1}))$. We minimize $\text{KL}[q(Z)||p(Z|Y)]$ by maximizing the *Evidence Lower Bound (ELBO)* (see App. A for derivation)

$$\log p(Y) \geq \mathbb{E}_{q(Z)} [\log p(Y|Z)] - \text{KL}[q(z(t_0))||p(z(t_0))]. \quad (6)$$

Since the transition kernel $p(z(t_n)|z(t_{n-1}))$ is identical for both $q(Z)$ and $p(Z)$, the term $\text{KL}[q(Z)||p(Z)]$ boils down to $\text{KL}[q(z(t_0))||p(z(t_0))]$, which is available in closed form for many pairs of distributions, such as two Gaussians. Contrarily, prior work [Li et al., 2020, Tzen & Raginsky, 2019] rather uses an approximate transition kernel $q(z(t_n)|z(t_{n-1}))$ governed by a different drift function $g(z(t))$ from the f_θ of the true transition kernel $p(z(t_n)|z(t_{n-1}))$ in the approximate posterior, resulting in a KL term $\text{KL}[q(Z)||p(Z)] = \mathbb{E}_{q(Z)} [\int \frac{1}{2} \|u(z(t))\|^2 dt]$. As opposed to our simple $\text{KL}[q(z(t_0))||p(z(t_0))]$, this expression is analytically intractable for most g and f_θ combinations, as $u(z(t))$ is defined only implicitly as $L_\phi(z(t))u(z(t)) = f_\theta(z(t)) - g(z(t))$.

Independently of the chosen transition kernel, the ELBO computation requires an accurate approximation of the data fit term $\mathbb{E}_{q(Z)} [\log p(Y|Z)]$ at affordable cost. This term involves calculating expectation of the log-likelihood with respect to the marginal approximate posterior $q(z(t_n))$ at each time point t_n when an observation is made, resulting in a series of nested integrals

$$\begin{aligned} q(z(t_n)) &= \int q(z_0)p(z(t_1)|z(t_0)) \dots p(z(t_n)|z(t_{n-1}))dz(t_0), \dots, z(t_{n-1}) \\ &= \int p(z(t_n)|z(t_{n-1})) \dots \underbrace{\left[\int p(z(t_1)|z(t_0))q(z(t_0))dz(t_0) \right]}_{q(z(t_1))} \dots dz(t_{n-1}). \end{aligned} \quad (7)$$

The above expression introduces two challenges: i) evaluating the transition kernel $p(z(t_{n+1})|z(t_n))$ and ii) solving the nested integral with respect to each $z(t_n)$. The transition kernel can be accessed by solving the Fokker–Planck–Kolmogorov (FPK) equation, which is a nonlinear PDE with an often intractable solution. We will derive an approximation to the marginal approximate posterior $q(z(t_n))$ in Sec. 3, which is specifically tailored towards neural nets, and then extend our method in Sec. 4 towards a deterministic variational inference method. Our deterministic prediction method is applicable independently of the training objective and can be applied at either training or test time.

3 Bidimensional Moment Matching

In this section we derive a novel deterministic solution to the nested marginal as defined in Eq. 7. We craft our solution in four steps: (i) discretizing the NSDE in Eq. 8, (ii) approximating the marginal process distribution at every time point as a normal density in Eq. 11, (iii) analytically marginalizing out the Wiener process noise from moment matching update rules in Eqs. 13 and 14, (iv) approximating the intractable terms in the moment calculations in Sec. 3.2, 3.3, and 3.4.

Instead of solving the FPK equation, we may obtain an approximation to the transition kernel $p(z(t_{n+1})|z(t_n))$ by firstly solving for the next state $z(t_{n+1})$ as in Eq. 3. Since the Wiener process injects randomness to any arbitrarily small time interval, the solution of any NSDE with drift and diffusion networks with at least one hidden layer is analytically intractable. In the following we refer to the discretized version of the continuous stochastic process $z(t_n)$ as z_k . For notational clarity, we assume a uniform discretization, though the choice of the time step size $\Delta t > 0$ is arbitrary and can be chosen dynamically if desired. As a numerical approximation to Eq. 3, we adopt the *Euler-Maruyama* (EM) method due to its computational efficiency, which follows the update rule

$$z_{k+1} := z_k + f_\theta(z_k)\Delta t + L_\phi(z_k)\Delta w_k, \quad (8)$$

where $\Delta w_k \sim \mathcal{N}(0, \Delta t)$. This solution amounts to the below approximation of the transition kernel

$$p(z_{k+1}|z_k) := \mathcal{N}(z_{k+1}|m_{k+1}(z_k), S_{k+1}(z_k)), \quad (9)$$

where $m_{k+1}(z_k) := z_k + f_\theta(z_k)\Delta t$ and $S_{k+1}(z_k) := L_\phi(z_k)L_\phi(z_k)^T\Delta t$ are the mean and variance of a normal density. Given the above approximation of the transition kernel, we may evaluate the marginal distribution of a discretized SDE by solving the recurrence relation below

$$p(z_{k+1}) = \int p(z_{k+1}|z_k)p(z_k)dz_k = \int \mathcal{N}(z_{k+1}|m_{k+1}(z_k), S_{k+1}(z_k))p(z_k)dz_k. \quad (10)$$

We will obtain a solution to our initial problem of calculating the marginal posterior at an arbitrary time point t_n , once we are able to evaluate the above recursion for any step k . Prior work [Tzen & Raginsky, 2019, Look & Kandemir, 2019, Li et al., 2020] evaluates this analytically intractable recurrence relation via MC integration. After sampling multiple trajectories from the discretized NSDE as defined in Eq. 8, the dependence on the previous time step z_k in Eq. 10 can be marginalized out. As we find out that sampling noise impairs the predictive calibration (see Fig. 1), our goal is derive a deterministic approximation of the intractable process distribution.

3.1 Assumed Process Density

As the marginal distribution of a discretized NSDE (Eq. 10) is also intractable for non-trivial architectures, we approximate the marginal at every step k by a normal density

$$p(z_k) \approx \mathcal{N}(z_k|\mu_k, \Sigma_k), \quad (11)$$

where $\mu_k := \mathbb{E}[z_k]$ and $\Sigma_k := \text{Cov}[z_k]$ are with respect to the stochastic process. This approximation simplifies the problem to calculating the first two moments of z_k . Plugging the assumed density in Eq. 11 into the recurrence relation for estimation of $p(z_{k+1})$, as defined in Eq. 10, amounts to approximating the marginal process distribution at every time point by matching moments progressively in time direction. We refer to this chain of operations as *Horizontal Moment Matching (HMM)*.

Calculating μ_{k+1} and Σ_{k+1} does not appear to be a simpler problem at the first sight than solving Eq. 10. However, it is possible to obtain a more pleasant expression by reparameterizing $p(z_{k+1})$ as

$$w_k \sim N(w_k|0, I), \quad z_k \sim \mathcal{N}(z_k|\mu_k, \Sigma_k), \quad z_{k+1} := z_k + f_\theta(z_k)\Delta t + L_\phi(z_k)\sqrt{\Delta t}w_k, \quad (12)$$

where I is the identity matrix with appropriate dimensionality. We arrive at the following alternative view of the first moment of $p(z_{k+1})$ using the law of the unconscious statistician

$$\mu_{k+1} = \mu_k + \mathbb{E}[f_\theta(z_k)]\Delta t. \quad (13)$$

The corresponding covariance reads

$$\begin{aligned} \Sigma_{k+1} = & \Sigma_k + \text{Cov}[f_\theta(z_k)]\Delta t^2 + \text{Cov}[f_\theta(z_k), z_k]\Delta t + \\ & \text{Cov}[f_\theta(z_k), z_k]^T\Delta t + \mathbb{E}[L_\phi(z_k)L_\phi^T(z_k)]\Delta t, \end{aligned} \quad (14)$$

where $\text{Cov}[f_\theta(z_k), z_k]$ denotes the cross-covariance between the random vectors in the arguments. Eq. 14 can be derived by integrating out the Wiener process and rewriting the expression according to the bilinearity of the covariance operator. See Appx. B for further details. Moment matching solutions along similar lines have been developed earlier for SDEs [Särkkä & Sarmavuori, 2013]. However, they have not yet been tailored for the specific needs of NSDEs.

3.2 Computing the drift network moments

After applying the HMM scheme, the terms $\mathbb{E}[f_\theta(z_k)]$ and $\text{Cov}[f_\theta(z_k)]$ amount to the first two moments of a random variable obtained by propagating $z_k \sim \mathcal{N}(\mu_k, \Sigma_k)$ through the neural net $f_\theta(z_k) = u_L(u_{L-1}(\dots u_2(u_1(z_k)) \dots))$, composed of a chain of L simple functions (layers), typically an alternation of affine transformations and nonlinear activations. Calculating the moments of $f_\theta(z_k)$ is analytically intractable due to the nonlinear activations. We approximate this computation by another round of moment matching, this time by propagating the input noise through the neural net. Denote the feature map at layer l at time step k as $h_k^l := u_l(u_{l-1}(\dots u_2(u_1(z_k)) \dots))$, which is a random variable due to z_k and is related recursively to the feature map of the previous layer as $h_k^l = u_l(h_k^{l-1})$. Denoting $h_k^0 := z_k$, we approximate the distributions on layers recursively as

$$h_k^l = u_l(h_k^{l-1}) \approx \tilde{h}_k^l \sim \mathcal{N}(a_k^l, B_k^l), \quad (15)$$

where $a_k^l := \mathbb{E}[u_l(\tilde{h}_k^{l-1})]$ and $B_k^l := \text{Cov}[u_l(\tilde{h}_k^{l-1})]$. We refer to applying this approximation throughout all neural net layers as *Vertical Moment Matching (VMM)*. We provide output moments a_k^L and B_k^L for commonly used layers in Appx. C. A similar approach has been applied earlier to *Bayesian Neural Nets* (BNN) for random weights in various contexts such as expectation propagation [Hernandez-Lobato & Adams, 2015, Ghosh et al., 2016], deterministic variational inference [Wu et al., 2019], and evidential deep learning [Haussmann et al., 2020]. To our knowledge, no prior work has applied this approach to propagating input uncertainty through a deterministic network in the dynamics modeling context. As an outcome of VMM, we get $\mathbb{E}[f_\theta(z_k)] \approx a_k^L$ and $\text{Cov}[f_\theta(z_k)] \approx B_k^L$.

3.3 Computing the diffusion network moments

We assume the diffusion matrix $L_\phi(z_k)$ to be diagonal for computational efficiency, though our method generalizes trivially to a full diffusion covariance. Overloading the notation for the sake of brevity, we denote an L -layer neural net assigned to its diagonal entries as $L_\phi(z_k) := v_L(v_{L-1}(\dots v_2(v_1(z_k)) \dots))$ with feature maps defined recursively as $e_k^l := v_l(e_k^{l-1})$. Following VMM, we pass the moments through the network simply by approximating the random (due to noisy z_k) feature map e_k^l by a normal distribution $\tilde{e}_k^l \sim \mathcal{N}(c_k^l, D_k^l)$ applying the moment matching rules to Eq. 15 literally on c_k^l and D_k^l and get as output $\mathbb{E}[L_\phi(z_k)L_\phi^T(z_k)] \approx (D_k^L + (c_k^L)(c_k^L)^T) \odot I := D_k$, with \odot denoting the Hadamard product. The second central moment D_k is a diagonal matrix due to the restriction of a vector-valued output of $L_\phi(z_k)$.

3.4Computing the cross-covariance

The term $\text{Cov}[f_\theta(z_k), z_k]$ stands for the cross-covariance between the input z_k , which is itself a random variable, and its transformation with the drift function $f_\theta(z_k)$. Due to the same reasons as the mean and covariance of $f_\theta(z_k)$, this cross-covariance term cannot be analytically calculated except for trivial drift functions. However, cross-covariance is not provided as a direct outcome of VMM. As being neither a symmetric nor a positive semi-definite matrix, inaccurate approximation of cross-covariance may impair numerical stability. This fact provides us yet another motivation for maintaining our method deterministic. Applying Stein's lemma [Liu, 1994]

$$\text{Cov}[z_k, f_\theta(z_k)] = \text{Cov}[z_k, z_k] \mathbb{E}[\nabla_{z_k} f_\theta(z_k)] \quad (16)$$

for the first time in the context of matching moments of a neural net, we obtain a form that is easier to approximate. The covariance $\text{Cov}[z_k, z_k]$ is provided from the previous time step as Σ_k , but the expected gradient $\mathbb{E}[\nabla_{z_k} f_\theta(z_k)]$ needs to be explicitly calculated. In standard BNN inference, where the source of uncertainty is the weights, we have the interchangeability property for the gradients with respect to the weight distribution parameters ξ as $\nabla_\xi \mathbb{E}_{q(\theta|\xi)}[f_\theta(z_k)] = \mathbb{E}_{q(\theta|\xi)}[\nabla_\xi f_\theta(z_k)]$. This trick is not applicable to our case as the gradient is with respect to z_k . In other words, $\mathbb{E}[\nabla_{z_k} f_\theta(z_k)]$ is not equal to $\nabla_{z_k} \mathbb{E}[f_\theta(z_k)]$, which would otherwise allow us to simply use $\nabla \mu_k$.

We define the Jacobian of a vector-variate function u with respect to its input z as $\nabla_z u(z)$. Applying the chain rule, the expectation of the derivative of a neural net with respect to a random input reads

$$\mathbb{E}[\nabla_{z_k} f_\theta(z_k)] = \mathbb{E}[\nabla_{h_k^{L-1}} u_L(h_k^{L-1}) \dots \nabla_{z_k} u_1(z_k)], \quad (17)$$

which is also analytically intractable. We facilitate computation by making the assumption that the mutual information between nonlinear feature maps of different layers is small

$$\int p(h_k^l, h_k^{l'}) \log \left\{ \frac{p(h_k^l, h_k^{l'})}{p(h_k^l)p(h_k^{l'})} \right\} dh_k^l dh_k^{l'} \approx 0, \quad (18)$$

for all pairs (l, l') with $l \neq l'$. Applying this assumption of decoupled activations on Eq. 17, we get

$$\mathbb{E}[\nabla_{z_k} f_\theta(z_k)] \approx \prod_{l=0}^{L-1} \mathbb{E}_{h_k^l} [\nabla_{h_k^l} u_{l+1}(h_k^l)]. \quad (19)$$

We test this assumption empirically by feeding a random input $z \sim N(0, I)$ into a neural net with two fully-connected and equally wide hidden layers. As depicted in Fig. 2, the nonlinear activation maps of different layers carry ignorable mutual information even for narrow architectures, e.g. 16 neurons. Mutual information shrinks fast when the hidden layers get wider and get ignorably small for widths relevant for practical use, such as 64 neurons. Despite being intractable, these expectations can be efficiently approximated by reusing the outcomes of the VMM step in Eq. 15 as follows

$$\mathbb{E}[\nabla_{h_k^l} u_{l+1}(h_k^l)] \approx \mathbb{E}_{\tilde{h}_k^l} [\nabla_{\tilde{h}_k^l} u_{l+1}(\tilde{h}_k^l)]. \quad (20)$$

We attain a deterministic approximation to Stein's lemma by taking the covariance Σ_k from VMM and the expected gradient from Eq. 20:

$$\begin{aligned} \text{Cov}[z_k, f_\theta(z_k)] &\approx \Sigma_k \prod_{l=0}^{L-1} \mathbb{E}_{\tilde{h}_k^l} [\nabla_{\tilde{h}_k^l} u_{l+1}(\tilde{h}_k^l)] \\ &:= C_k. \end{aligned} \quad (21)$$

We provide the expected gradient

$\mathbb{E}_{\tilde{h}_k^l} [\nabla_{\tilde{h}_k^l} u_{l+1}(\tilde{h}_k^l)]$ for commonly used layer types in Appx. C.

4 Deterministic Variational Inference for NSDEs

The main difficulty in the ELBO computation is to approximate the intractable data fit term as accurately as possible at low computational cost. Below we present the methodological highlights of our novel deterministic method to evaluate this term accurately and affordably and refer the reader to Appx. D for its algorithmic details. For notational simplicity consider the equally spaced time series $Y = \{y(t_1), \dots, y(t_N)\}$ with step size Δt , the data fit term reads in full detail as

$$\mathbb{E}_{q(Z)} [\log p(Y|Z)] = \sum_{n=1}^N \int \log p(y(t_n)|z(t_n)) \underbrace{p(z(t_n)|z(t_{n-1}))q(z(t_{n-1}))}_{q(z(t_n))} dz(t_{n-1}). \quad (22)$$

We obtain the marginal approximate posterior $q(z(t_n)) = q(z_k)$ by propagating moments along the time direction with BMM as

$$\mu_{k+1} := \mu_k + a_k^L \Delta t, \quad \Sigma_{k+1} := \Sigma_k + B_k^L \Delta t^2 + (C_k + C_k^T) \Delta t + D_k \Delta t, \quad (23)$$

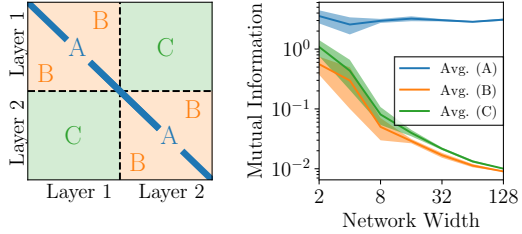


Figure 2: Nonlinear activations get statistically independent as the network width increases, supporting our assumption in Eq. 19. Imagine a matrix containing mutual information between all pairs of nonlinear activations h_k^l in a two-hidden-layer neural net as in the left panel. Group its entries into blocks: the diagonal block (A) giving the entropy of an activation, the within-layer off-diagonal block (B) giving the dependence of sibling activations, the cross-layer off-diagonal (C) giving the dependence of activations in different layers. As seen in the right panel, the average mutual information in blocks (B) and (C) decreases sharply with increasing layer width. Solid lines and shaded area represent average mutual information and its standard deviation over 100 repetitions.

where μ_0 and Σ_0 are given by $q(z(t_0))$. In the above expression we use $a_k^L \approx \mathbb{E}[f_\theta(z_k)]$, $B_k^L \approx \text{Cov}[f_\theta(z_k)]$, and $D_k \approx \mathbb{E}[L_\phi(z_k)L_\phi^T(z_k)]$, which are obtained from VMM. The term $C_k \approx \text{Cov}[z_k, f_\theta(z_k)]$ is obtained via Stein’s lemma. Plugging the above approximation into the expression for calculating the marginal likelihood in Eq. 22, we obtain

$$\int \log p(y(t_n)|z(t_n))q(z(t_n))dz(t_n) \approx \int \log p(y_k|z_k)\mathcal{N}(z_k|\mu_k, \Sigma_k)dz_k, \quad (24)$$

which can be closely approximated for common likelihood functions such as the logistic or softmax mapping [Daunizeau, 2017]. Alternatively, the moments can be approximated by VMM for a neural observation model with mean and covariance depending on z_k . The BMM algorithm is directly applicable at the test time in approximation of the posterior predictive distribution of a new sample $Y^* = \{y^*(t_{N+1}), \dots, y^*(t_{N+M})\}$ as follows:

$$\begin{aligned} p(Y^*|Y) &= \int p(Y^*|Z)p(Z|Y)dZ \approx \int p(Y^*|Z)q(Z)dZ \\ &= \int \dots p(y^*(t_{N+1})|z(t_{N+1})) \underbrace{\left[\int p(z(t_{N+1})|z(t_N))q(z(t_N))dz(t_N) \right]}_{q(z(t_{N+1}))} \dots dz(t_{N+M}). \end{aligned} \quad (25)$$

5 Experiments

We provide first an empirical investigation of our BMM algorithm, and then benchmark against recent stochastic time series approaches on a synthetic environment with nonlinear dynamics and two challenging real-world time series forecasting applications.

5.1 Numerical properties

We investigate the numerical properties of the BMM algorithm in terms of integration error, computation cost, and generalization to multiple modes. We also compare cubature as an alternative choice to VMM, which is a standard numerical method for approximating the expectation of a smooth function with respect to a multivariate normal distribution. See Appx. E for details. We find out that VMM has favorable computational properties over cubature.

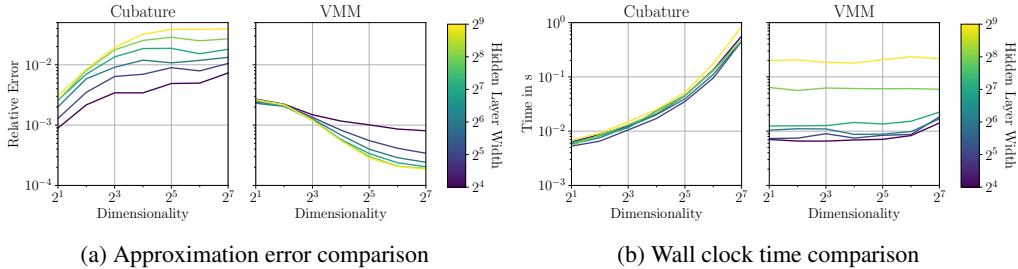


Figure 3: Comparison of VMM versus cubature in terms of approximation error and computation time. We generate a randomly initialized neural net $f_\theta(x)$. The dimensionalities of x and $f_\theta(x)$ are equal and vary in the horizontal axis. The neural net $f_\theta(x)$ has three fully-connected layers of varying widths color-coded according to the heatmap on the right of the figures, ReLU activation, and dropout with rate 0.2. As cubature cannot handle a random $f_\theta(x_k)$ and discontinuous activations, we evaluate it with tanh activation and without dropout. We aim to approximate the intractable expectation $r = \int f_\theta(x)\mathcal{N}(x|\tilde{\mu}, \tilde{\Sigma})dx$, where $\tilde{\mu} \sim \mathcal{N}(0, I)$ and $\tilde{\Sigma} \sim \mathcal{W}(I, \dim(I))$ with Wishart distribution \mathcal{W} . We repeat the experiment 512 times and report the average relative error $\|r - \hat{r}\|^2/\|r\|^2$ in Panel (a), where r is represented by averaging over 10 million Monte Carlo simulations and \hat{r} is approximated via cubature and VMM, respectively. We calculate the computation time of this experiment in all repetitions and report its average as a function of input dimensionality in Panel (b).

Approximation Error. In Fig. 3a, we compare VMM and cubature in approximating $\mathbb{E}[f_\theta(z)]$ for a normal distributed input z and the effect of neural net width and input/output dimensionality

on approximation accuracy. For low dimensionalities, the relative error of VMM is approximately equal to cubature. The approximation error of VMM shrinks with increasing hidden layer width and dimensionality. This is expected since summing a larger number of decorrelated variables makes the assumption of normally distributed intermediate activations more accurate due to the central limit theorem [Wang & Manning, 2013].

Computational Cost. Propagation of S particles with dimensionality D along K time steps requires $\mathcal{O}(SKH^2)$ compute, when dynamics is governed by a NSDE with hidden layer width $H \geq D$. The computational cost of the NSDE is governed by the cost of the $H \times H$ -dimensional transformation in the hidden layer, which requires $\mathcal{O}(H^2)$ compute. Our method BMM approximates the $S \rightarrow \infty$ limit, while requiring only $\mathcal{O}(KH^3)$ compute. The additional factor H arises due to the approximation cost of the quadratic covariance. Replacing VMM with cubature in our framework results in an algorithm requiring $\mathcal{O}(KDH^2 + KD^3)$ compute. Cubature requires at least $\mathcal{O}(D)$ NSDE evaluations, which causes the additional factor D in the first term. The second term arises from the Cholesky decomposition of the input. We visualize in Fig. 3b the wall clock of VMM and cubature as a function of dimensionality and hidden layer width. Dimensionality sets a bottleneck for cubature, while it barely affects VMM. Contrarily, VMM gets significantly slower as the hidden layer width increases, while the computational cost of cubature remains similar. VMM is adaptable to setups requiring high learning capacity by building narrow and deep architectures. However, dimensionality of the time series signal is an external factor that limits the applicability of cubature.

Multimodal Processes. Our method can generalize to multiple modes under mild assumptions. If training sequences come with the knowledge of the modality, a separate unimodal NSDE can be fit to each mode and their mixture can be used during prediction. If modality assignments are not known a-priori, an initial clustering step can be applied. We visualize prediction results in Fig. 4 on the bimodal double-well dynamics, after clustering the training data and training a separate NSDE on each mode. BMM can also serve as a subroutine in more complex design, such as deterministic variational inference of a Dirichlet process mixture model [Nieto-Barajas & Contreras-Cristan, 2014].

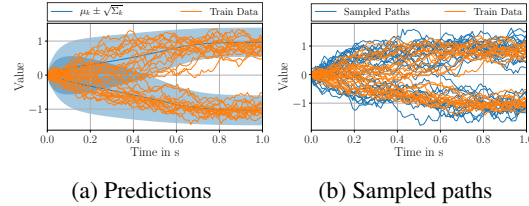


Figure 4: Handling multimodality with a NSDE applied to double-well potential dynamics: $dx_t = 4x_t(1 - x_t^2)dt + dw_t$. We train a separate model on each mode and predict with BMM in Panel (a), and with NSDE-MC in Panel (b).

5.2 Benchmarks

We benchmark on three different time series prediction datasets that enable a comparison to the state of the art methods for learning-based modeling of stochastics. See Appx. F for experimental details.

Datasets. We benchmark on three data sets: (i) The stochastic Lotka-Volterra dynamics as a challenging nonlinear dynamical system, (ii) The Beijing air quality dataset [Zhang et al., 2017] containing a high-dimensional sequence of hourly measurements of particle concentrations, temperature, and other features at three different locations, (iii) The 3-DOF-Robot dataset [Agudelo-España et al., 2020] consisting of measurements on a three degree-of-freedom real robot arm, which was recorded at two separate operating modes, low frequency (IID) and high frequency (Transfer). The real world data sets are challenging forecasting tasks due to measurement noise and nonlinear dynamics.

Baselines. Our baselines represent the state of the art of SDE based dynamics modeling. We benchmark our method (BMM) against: (i) *NODE* [Chen et al., 2018]: Neural ODE, hence NSDE without diffusion, (ii) *NSDE-MC* [Li et al., 2020]: Monte Carlo sampling-based prediction with NSDE, (iii) *diffWGP* [Jorgensen et al., 2020]: A SDE with drift and diffusion modeled as the predictive mean and covariance of a sparse GP, the state of the art of differential equation modeling with GPs, (iv) *Cubature*: A variant of ours using cubature in place of VMM. We train NSDE variants by maximizing the ELBO in Eq. 6 and provide network architectures in Appx. H.

Evaluation Criteria. We evaluate BMM against the baselines with respect to prediction accuracy by *Mean Squared Error (MSE)* and uncertainty calibration by *Negative Log-Likelihood (NLL)* and

Expectation of Coverage Probability Error (ECPE) [Cui et al., 2020]. ECPE measures the calibration as the absolute difference between the true and predicted frequency of data. See Appx. G for details.

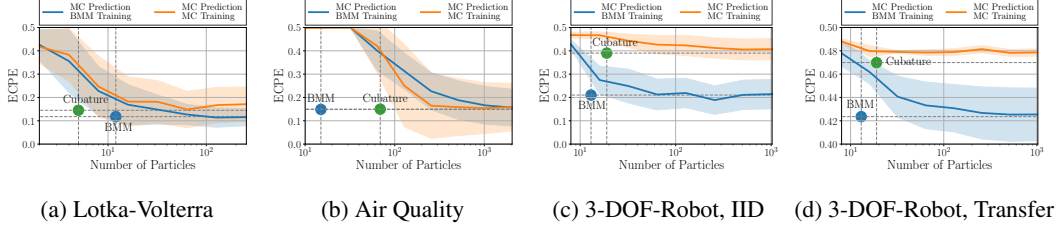


Figure 5: Cost-benefit analysis of calibration with different methods. One particle is equal to one MC simulation along a trajectory. BMM is our proposed method, Cubature is our method with cubature as a replacement for VMM, the orange line is training and prediction with MC sampling, and the blue line is training with our method and prediction with MC sampling. In all four data sets, the minimum calibration error is achieved with low computational cost if our deterministic method is used for both training and prediction. We show mean and standard deviation over 10 runs.

Table 1: Forecasting results for: (i) Lotka-Volterra (2 dimensions, 100 time steps), (ii) Air Quality (34 dimensions, 47 time steps), and (iii) 3-DOF-Robot (9 output dimensions, 3 input dimensions, 100 time steps). We provide average and standard error over 10 runs.

Model	Lotka-Volterra		Air Quality		3-DOF-Robot			
	MSE	NLL	MSE	NLL	IID		Transfer	
NODE [Chen et al., 2018]	1.98 ± 0.04	-	1.85 ± 0.15	-	0.22 ± 0.01	-	29.78 ± 1.66	-
diffWGP [Jorgensen et al., 2020]	-	-	2.39 ± 0.04	46.92 ¹ ± 0.75	-	-	-	-
NSDE-MC [Li et al., 2020]	2.07 ± 0.11	4.95 ± 0.44	1.90 ± 0.07	43.84 ± 0.75	0.22 ± 0.02	21.69 ± 1.75	30.52 ± 1.97	1821 ± 12
NSDE-Cubature (Ours, Ablation)	1.91 ± 0.08	4.84 ± 0.19	1.45 ± 0.04	37.84 ± 0.39	0.22 ± 0.02	5.65 ± 0.33	31.32 ± 1.89	352 ± 27
NSDE-BMM (Ours, Proposed)	1.75 ± 0.03	4.35 ± 0.15	1.44 ± 0.10	34.38 ± 0.50	0.16 ± 0.01	7.27 ± 1.31	12.31 ± 1.16	102 ± 12

Results. As shown in Tab. 1, BMM outperforms all baselines in all data sets with respect to both NLL and MSE, with the only exception of NLL in the 3-DOF-Robot (IID) data set where it comes behind Cubature. We attribute the improved prediction accuracy of BMM over cubature to its reduced approximation error, as demonstrated in Fig. 3a. BMM proves to make more accurate predictions than both NSDE-MC and diffWGP probably due to the improved stability of the training process thanks to its deterministic objective. This outcome is despite the fact that diffWGP models the diffusion as a Wishart process, while BMM uses a diagonal diffusion function.

We present Fig. 5 as our main result: *The BMM algorithm reaches a level of uncertainty calibration, which is prohibitively costly for MC sampling.* In all three applications, MC sampling requires more than 50 roll-outs to match the ECPE, which our deterministic BMM provides. BMM is separately applicable at training and prediction times. We find out that BMM improves on MC sampling in the 3-DOF-Robot data set even when used only for training, as visible from the blue curves in Fig. 5c and 5d being much steeper than the orange curves. We skip the MC training and BMM prediction variant, as it is already represented by the right extreme of the orange curves. We observe BMM to bring smaller ECPE than cubature in three of the four plots at comparable computational cost.

6 Conclusion and Broader Impact

We proposed a computationally efficient and deterministic VI algorithm, which also enables accurate uncertainty quantification at moderate computational cost. We present a general-purpose methodological contribution, which is applicable beyond the use cases demonstrated in our experiments. Examples include vehicle behavior prediction, stock price forecasting, and system identification for robot manipulation. While our method improves the reliability of predictive uncertainties, it does not contribute significantly to the explainability of the inferred system dynamics, which could be a risk

¹After correspondence with the authors, we present in this paper the correct NLL for diffWGP. In the original paper, an unknown issue caused a shift of the NLL.

factor in safety-critical applications. Furthermore, in potential use of our findings in fairness-sensitive applications, such as customer segmentation or crime forecasting, it should be accompanied with the recent findings of fairness research.

References

- Abbati, G., Wenk, P., Osborne, M., Krause, A., Schölkopf, B., and Bauer, S. AReS and MaRS Adversarial and MMD-Minimizing Regression for SDEs. In *ICML*. 2019.
- Agudelo-España, D., Zadaianchuk, A., Wenk, P., Garg, A., Akpo, J., Grimminger, F., Viereck, J., Naveau, M., Righetti, L., Martius, G., Krause, A., Schölkopf, B., Bauer, S., and Wüthrich, M. A Real-Robot Dataset for Assessing Transferability of Learned Dynamics Models . In *ICRA*. 2020.
- Archambeau, C., Cornford, D., Oppen, M., and S.-Taylor, J. Gaussian Process Approximations of Stochastic Differential Equations. *Proceedings of Machine Learning Research*, 1, 2007.
- Bensimhou, M. N-Dimensional cumulative function, and other useful facts about Gaussians and normal densities. 2013.
- Chen, T. Q., Rubanova, Y., Bettencourt, J., and Duvenaud, D. K. Neural Ordinary Differential Equations. In *NeurIPS*. 2018.
- Cui, P., Hu, W., and Zhu, J. Calibrated Reliable Regression using Maximum Mean Discrepancy. In *NeurIPS*. 2020.
- Daunizeau, J. Semi-analytical approximations to statistical moments of sigmoid and softmax mappings of normal variables. *ArXiv*, abs/1703.00091, 2017.
- Gal, Y. and Ghahramani, Z. Dropout as a Bayesian Approximation: Representing Model Uncertainty in Deep Learning. In *ICML*. 2016.
- Ghosh, S., Fave, F., Delle, M., and Yedidia, J. Assumed Density Filtering Methods for Learning Bayesian Neural Networks. In *AAAI*. 2016.
- Haussmann, M., Gerwinn, S., and Kandemir, M. Bayesian Evidential Deep Learning with PAC Regularization, 2020.
- Hegde, P., Heinonen, M., Lähdesmäki, H., and Kaski, S. Deep learning with differential Gaussian process flows. In *AISTATS*. 2019.
- Hernandez-Lobato, J. M. and Adams, R. Probabilistic Backpropagation for Scalable Learning of Bayesian Neural Networks. In *ICML*. 2015.
- Jorgensen, M., Deisenroth, M. P., and Salimbeni, H. Stochastic Differential Equations with Variational Wishart Diffusions. In *ICML*. 2020.
- Kingma, D. P. and Ba, J. Adam: A Method for Stochastic Optimization. In *ICLR*. 2015.
- Kuleshov, V., Fenner, N., and Ermon, S. Accurate Uncertainties for Deep Learning Using Calibrated Regression. In *ICML*. 2018.
- Li, X., Wong, T. L., Chen, R. T. Q., and Duvenaud, D. Scalable Gradients for Stochastic Differential Equations. In *AISTATS*. 2020.
- Liu, J. S. Siegel’s formula via Stein’s identities. *Statistics & Probability Letters*, 21, 1994.
- Look, A. and Kandemir, M. Differential Bayesian Neural Networks. In *NeurIPS Workshop Bayesian Deep Learning*. 2019.
- Nieto-Barajas, L. E. and Contreras-Cristan, A. A Bayesian Nonparametric Approach for Time Series Clustering. *Bayesian Analysis*, 0, 2014.
- Oksendal, B. *Stochastic Differential Equations: An Introduction with Applications*. Springer, 1992.

- Paszke, A., Gross, S., Chintala, S., Chanan, G., Yang, E., DeVito, Z., Lin, Z., Desmaison, A., Antiga, L., and Lerer, A. Automatic differentiation in pytorch. In *NeurIPS*. 2017.
- Platt, J. C. Probabilistic Outputs for Support Vector Machines and Comparisons to Regularized Likelihood Methods. In *Advances in Large Margin Classifiers*. 1999.
- Ryder, T., Golightly, A., McGough, A. S., and Prangle, D. Black-Box Variational Inference for Stochastic Differential Equations. In *ICML*. 2018.
- Särkkä, S. and Sarmavuori, J. Gaussian filtering and smoothing for continuous-discrete dynamic systems. *Signal Processing*, 93, 2013.
- Särkkä, S. and Solin, A. *Applied Stochastic Differential Equations*. Cambridge University Press., 2019.
- Thiagarajan, J. J., Venkatesh, B., Sattigeri, P., and Bremer, P. Building Calibrated Deep Models via Uncertainty Matching with Auxiliary Interval Predictors. In *AAAI*. 2020.
- Titsias, M. and Lawrence, N. D. Bayesian Gaussian Process Latent Variable Model. In *ICML*. 2010.
- Tzen, B. and Raginsky, M. Neural Stochastic Differential Equations: Deep Latent Gaussian Models in the Diffusion Limit. *ArXiv*, abs/1905.09883, 2019.
- Wan, E. A. and Merwe, R. V. D. The Unscented Kalman Filter for Nonlinear Estimation. 2000.
- Wang, S. and Manning, C. Fast dropout training. In *ICML*. 2013.
- Wu, A., Nowozin, S., Meeds, E., Turner, R. E., Hernandez-Lobato, J. M., and Gaunt, A. L. Deterministic Variational Inference for Robust Bayesian Neural Networks. In *ICLR*. 2019.
- Zhang, S., Bin, G., Anlan, D., Jing, H., Ziping, X., and Xi, C. S. Cautionary tales on air-quality improvement in Beijing. *Proceedings of the Royal Society: Mathematical, Physical and Engineering Sciences*, 473, 2017.

A Derivation of ELBO

Suppose $Y = \{y(t_1), \dots, y(t_N)\}$ to be a time series of length N observed at arbitrarily-spaced time points t_1, \dots, t_N with latent states $Z = \{z(t_0), z(t_1), \dots, z(t_N)\}$. During parameter inference we are interested in the true posterior $p(Z|Y)$, which is available via Bayes' law. Due to the intractability of $p(Z|Y)$ we resort to VI and define the approximate posterior as

$$q(Z) = q(z(t_0)) \prod_{n=1}^N p(z(t_n)|z(t_{n-1})). \quad (26)$$

We minimize the KL-divergence between $p(Z|Y)$ and $q(Z)$ by maximizing the ELBO

$$\begin{aligned} \log p(Y) &= \log \int p(Y|Z)p(Z) \frac{q(Z)}{p(Z)} dZ \\ &= \log \mathbb{E}_{q(Z)} \left[\frac{p(Y|Z)p(Z)}{q(Z)} \right] \\ &\geq \mathbb{E}_{q(Z)} \left[\log \frac{p(Y|Z)p(Z)}{q(Z)} \right] \\ &= \mathbb{E}_{q(Z)} [\log p(Y|Z)] - \mathbb{E}_{q(Z)} \left[\log \frac{q(Z)}{p(Z)} \right] \\ &= \mathbb{E}_{q(Z)} [\log p(Y|Z)] - \mathbb{E}_{q(Z)} \left[\log \frac{q(z(t_0)) \prod_{n=1}^N p(z(t_n)|z(t_{n-1}))}{p(z(t_0)) \prod_{n=1}^N p(z(t_n)|z(t_{n-1}))} \right] \\ &= \mathbb{E}_{q(Z)} [\log p(Y|Z)] - \mathbb{E}_{q(Z)} \left[\log \frac{q(z(t_0))}{p(z(t_0))} \right] \\ &= \mathbb{E}_{q(Z)} [\log p(Y|Z)] - \text{KL} [q(z(t_0)) || p(z(t_0))]. \end{aligned}$$

B Derivation of Mean and Covariance for Horizontal Moment Matching

We approximate the transition density at an arbitrary time step as $p_{\theta, \phi}(z_{k+1}|z_k) \approx \mathcal{N}(z_{k+1}|\mu_{k+1}, \Sigma_{k+1})$. By reparameterizing $p_{\theta, \phi}(z_{k+1}|z_k)$ we obtain

$$w_k \sim N(w_k|0, I), \quad z_k \sim \mathcal{N}(z_k|\mu_k, \Sigma_k),$$

$$z_{k+1} := z_k + f_{\theta}(z_k)\Delta t + L_{\phi}(z_k)\sqrt{\Delta t}w_k,$$

where I is the identity matrix with the dimensionality appropriate for the context. Mean μ_{k+1} and covariance Σ_{k+1} at time step $k+1$ can be expressed as

$$\mu_{k+1} = \mu_k + \mathbb{E}[f_{\theta}(z_k)]\Delta t.$$

$\Sigma_{k+1} = \Sigma_k + \text{Cov}[f_{\theta}(z_k)]\Delta t^2 + \text{Cov}[f_{\theta}(z_k), z_k]\Delta t + \text{Cov}[f_{\theta}(z_k), z_k]^T \Delta t + \mathbb{E}[L_{\phi}(z_k)L_{\phi}^T(z_k)]\Delta t$, where $\text{Cov}[f_{\theta}(z_k), z_k]$ denotes the cross-covariance between the random vectors in the arguments. In order to derive this result we hinge on [Särkkä & Solin \[2019\]](#) (pg. 174 Eq. 9.32 and 9.33), in which analytical solutions to SDEs by inserting a discretization scheme are proposed. Using the law of the unconscious statistician we obtain for the next mean

$$\begin{aligned} \mu_{k+1} &= \mathbb{E}[z_k + f_{\theta}(z_k)\Delta t + L_{\phi}(z_k)\sqrt{\Delta t}w_k] = \mu_k + \mathbb{E}[f_{\theta}(z_k)\Delta t] + \underbrace{\mathbb{E}[L_{\phi}(z_k)\sqrt{\Delta t}w_k]}_{=0} \\ &= \mu_k + \mathbb{E}[f_{\theta}(z_k)\Delta t]. \end{aligned}$$

In order to derive a tractable expression for the next covariance $\Sigma_{k+1} = \mathbb{E}[z_{k+1}z_{k+1}^T] - \mathbb{E}[z_{k+1}]\mathbb{E}[z_{k+1}]^T$ we first evaluate the expectation $\mathbb{E}[z_{k+1}z_{k+1}^T]$

$$\begin{aligned} \mathbb{E}[z_{k+1}z_{k+1}^T] &= \mathbb{E}[(z_k)(z_k)^T + (z_k)(f_{\theta}(z_k)\Delta t)^T + (z_k)(L_{\phi}(z_k)\sqrt{\Delta t}w_k)^T + (f_{\theta}(z_k)\Delta t)(z_k)^T + \\ &\quad (f_{\theta}(z_k)\Delta t)(f_{\theta}(z_k)\Delta t)^T + (f_{\theta}(z_k)\Delta t)(L_{\phi}(z_k)\sqrt{\Delta t}w_k)^T + \\ &\quad (L_{\phi}(z_k)\sqrt{\Delta t}w_k)(z_k)^T + (L_{\phi}(z_k)\sqrt{\Delta t}w_k)(f_{\theta}(z_k)\Delta t)^T + \\ &\quad (L_{\phi}(z_k)\sqrt{\Delta t}w_k)(L_{\phi}(z_k)\sqrt{\Delta t}w_k)^T] \\ &= \mathbb{E}[(z_k + f_{\theta}(z_k)\Delta t)(z_k + f_{\theta}(z_k)\Delta t)^T] + \mathbb{E}[(L_{\phi}(z_k))(L_{\phi}(z_k))^T]\Delta t, \end{aligned}$$

since $\mathbb{E}[w_k] = 0$ and $\mathbb{E}[w_k w_k^T] = I$. Using the bilinearity of the covariance operator we obtain

$$\begin{aligned}\Sigma_{k+1} &= \mathbb{E}[(z_k + f_\theta(z_k)\Delta t)(z_k + f_\theta(z_k)\Delta t)^T] - \mathbb{E}[(z_k + f_\theta(z_k)\Delta t)]\mathbb{E}[(z_k + f_\theta(z_k)\Delta t)^T] + \\ &\quad \mathbb{E}[(L_\phi(z_k))(L_\phi(z_k))^T]\Delta t \\ &= \text{Cov}(z_k + f_\theta(z_k)\Delta t) + \mathbb{E}[L_\phi(z_k)L_\phi^T(z_k)]\Delta t \\ &= \text{Cov}(z_k) + \text{Cov}(z_k, f_\theta(z_k)\Delta t) + \text{Cov}(f_\theta(z_k)\Delta t, z_k) + \text{Cov}(f_\theta(z_k)\Delta t) + \\ &\quad \mathbb{E}[L_\phi(z_k)L_\phi^T(z_k)]\Delta t.\end{aligned}$$

C Layers for BMM

Given the VMM output of the previous layer as $\tilde{h}_k^l \sim \mathcal{N}(a_k^l, B_k^l)$, we show below how these expressions can be calculated for three common layer types: (i) linear activations, (ii) nonlinear activations, and (iii) dropout. We provide a detailed discussion about the validity of the dropout layer for NSDEs and its usage as a whitening operation in order to tighten the Gaussian assumption.

C.1 Linear activations

The moments of an affine transformation $u_{l+1}(\tilde{h}_k^l) = W^{l+1}\tilde{h}_k^l + b^{l+1}$ are tractable as

$$\begin{aligned}\mathbb{E}[u_{l+1}(\tilde{h}_k^l)] &= W^{l+1}a_k^l + b^{l+1}, \\ \text{Cov}[u_{l+1}(\tilde{h}_k^l)] &= W^{l+1}B_k^l(W^{l+1})^T,\end{aligned}\tag{27}$$

where W^{l+1} and b^{l+1} correspond to the weights and bias of layer $l+1$. The expected gradient is then a constant

$$\mathbb{E}[\nabla_{\tilde{h}_k^l} u_{l+1}(\tilde{h}_k^l)] = W^{l+1}.\tag{28}$$

C.2 Nonlinear activations

The output moments of nonlinear activations are analytically not tractable. However, for many types of nonlinearities in widespread use, there exist tight approximations. For instance, the output moments of the ReLU activation $u_{l+1}(\tilde{h}_k^l) = \max(0, \tilde{h}_k^l)$, with $\tilde{h}_k^l \sim \mathcal{N}(a_k^l, B_k^l)$, function can be estimated as [Wu et al. \[2019\]](#)

$$\begin{aligned}\mathbb{E}[u_{l+1}(\tilde{h}_k^l)] &= \sqrt{\text{diag}(B_k^l)} \text{SR}\left(a_k^l / \sqrt{\text{diag}(B_k^l)}\right), \\ \text{Cov}[u_{l+1}(\tilde{h}_k^l)] &= \sqrt{\text{diag}(B_k^l)}(B_k^l)^T F(a_k^l, B_k^l),\end{aligned}$$

with $F(a_k^l, B_k^l) = (A(a_k^l, B_k^l) + \exp - Q(a_k^l, B_k^l))$. We introduce the dimensionless variable $\epsilon_k^l = a_k^l / \sqrt{\text{diag}(B_k^l)}$ and obtain $\text{SR}(\epsilon_k^l) = (\phi(\epsilon_k^l) + \epsilon_k^l \Phi(\epsilon_k^l))$, with ϕ and Φ representing the standard normal PDF and CDF. We take $\sqrt{\cdot}$ elementwise in this expression. The matrix valued function $A(a_k^l, B_k^l)$ is estimated as

$$A(a_k^l, B_k^l) = \text{SR}(\epsilon_k^l)\text{SR}(\epsilon_k^l)^T + \rho_k^l \Phi(\epsilon_k^l)\Phi(\epsilon_k^l)^T,\tag{29}$$

with $\rho_k^l = B_k^l / \left(\sqrt{\text{diag}(B_k^l)}\sqrt{\text{diag}(B_k^l)^T}\right)$. The i, j -th element of $Q(a_k^l, B_k^l)$ can be estimated as:

$$\begin{aligned}Q(a_k^l, B_k^l)_{i,j} &= -\log\left(\frac{g_{k_{i,j}}^l}{2\pi}\right) + \frac{\rho_{k_{i,j}}^l}{2g_{k_{i,j}}^l(1 + \bar{\rho}_{k_{i,j}}^l)}\left((\epsilon_{k_i}^l)^2 + (\epsilon_{k_j}^l)^2\right) - \\ &\quad \frac{\arcsin(\rho_{k_{i,j}}^l) - \rho_{k_{i,j}}^l}{\rho_{k_{i,j}}^l g_{k_{i,j}}^l} \epsilon_{k_i}^l \epsilon_{k_j}^l + \mathcal{O}((\epsilon_k^l)^4),\end{aligned}\tag{30}$$

with $g_k^l = \arcsin(\rho_k^l) + \rho_k^l \oslash (1 + \bar{\rho}_k^l)$, and $\bar{\rho}_k^l = \sqrt{1 - \rho_k^l \odot \rho_k^l}$. We denote with \odot elementwise division.

Since activation functions are applied element-wise, off-diagonal entries of the expected gradient are zero. The diagonal of the Jacobian of the ReLU function is the Heaviside step function [Wu et al. \[2019\]](#)

$$\text{diag} \left(\mathbb{E} \left[\nabla_{\tilde{h}_k^l} u_{l+1}(\tilde{h}_k^l) \right] \right) \approx \Phi \left(a_k^l / \sqrt{\text{diag}(B_k^l)} \right). \quad (31)$$

C.3 Dropout

Dropout is defined as the mapping $u_{l+1}(\tilde{h}_k^l) := \tilde{h}_k^l \odot \beta_k^l / q$ for a random vector β_k^l consisting of Bernoulli(q) distributed entries. The moments of which are available as

$$\begin{aligned} \mathbb{E}[u_{l+1}(\tilde{h}_k^l)] &= a_k^l, \\ \text{Cov}[u_{l+1}(\tilde{h}_k^l)] &= B_k^l + \text{diag} \left(\frac{1-q}{q} (B_k^l + (a_k^l)(a_k^l)^T) \right). \end{aligned} \quad (32)$$

C.3.1 Dropout tightens the Gaussian assumption

As shown in the above equations, dropout increases the value of the diagonal entries in the covariance matrix compared to the off-diagonal entries. Consequently, dropout is helpful to decorrelate the co-variables of a layer, making their sum approach the normal distribution due to the *Central Limit Theorem (CLT)*. We demonstrate in Fig. 6a the influence of the Dropout layer. We find it mild to assume a neural net layer to be wider than 20 neurons, which is sufficient for CLT to give an accurate approximation for practical purposes.

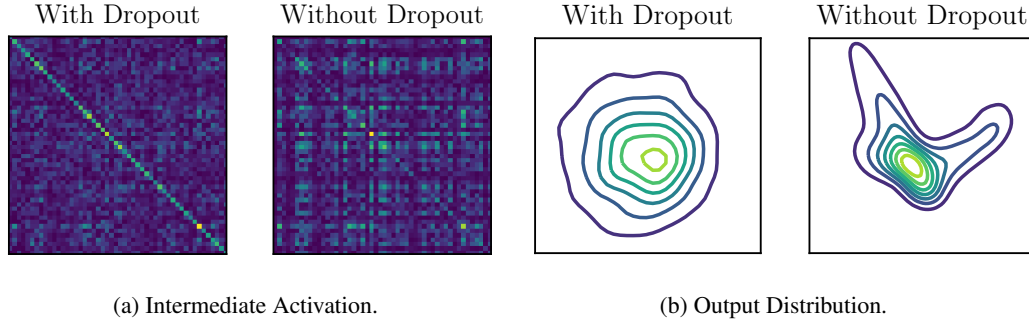


Figure 6: Dropout decorrelates the activation map. We pass a multivariate normal distributed random vector through a neural net with three 50-neuron-wide hidden layers with ReLU activation. The off-diagonals of the covariance matrix of the activation map are suppressed when dropout is used after each ReLU activation, as shown in Panel (a) for an intermediate layer and Panel (b) for the output layer. Decorrelation of a large number of co-variables makes a normal distribution an accurate approximation on their sum due to the central limit theorem.

C.3.2 Is Dropout a valid layer for NSDEs?

We may interpret dropout as a Bayesian approximation of the network parameters [\[Gal & Ghahramani, 2016\]](#). Doing so we may rewrite the original SDE as

$$\begin{aligned} \theta &\sim p(\theta(t)|\zeta), \phi \sim p(\phi(t)|\xi) \\ dz(t) &= f_{\theta(t)}(z(t)) dt + L_{\phi(t)}(z(t)) dw(t) \end{aligned}$$

Above the parameters θ and ϕ are time depending, i.e. we sample a new pair of $\theta(t)$ and $\phi(t)$ at each t . As the parameters are iid distributed across time the moment matching update rule is updated to

$$\begin{aligned} \mu_{k+1} &= \mu_k + \mathbb{E}_{z_k, \theta_k} [f_{\theta_k}(z_k)] \Delta t. \\ \Sigma_{k+1} &= \Sigma_k + \mathbb{E}_{\theta_k} [\text{Cov}[f_{\theta_k}(z_k)]] \Delta t^2 + \mathbb{E}_{\theta} [\text{Cov}[f_{\theta_k}(z_k), z_k]] \Delta t + \\ &\quad \mathbb{E}_{\theta_k} [\text{Cov}[f_{\theta_k}(z_k), z_k]^T] \Delta t + \mathbb{E}_{z_k, \phi_k} [L_{\phi_k}(z_k) L_{\phi_k}^T(z_k)] \Delta t. \end{aligned}$$

Above we marginalize out the introduced parameter uncertainty, which we can do efficiently by our proposed BMM algorithm. With this reinterpretation of dropout we obtain a deterministic drift and diffusion function for given set of parameters, which makes dropout consequently a valid layer.

C.3.3 Derivation of Moments

In order to derive these expressions we omit for simplicity the rescaling by q . Using independence between \tilde{h}_k^l and β_k^l we obtain straightforwardly $\mathbb{E}[u_{l+1}(\tilde{h}_k^l)]$

$$\mathbb{E}[u_{l+1}(\tilde{h}_k^l)] = \mathbb{E}[\tilde{h}_k^l \odot \beta_k^l] = \mathbb{E}[\tilde{h}_k^l] \mathbb{E}[\beta_k^l] = q \mathbb{E}[h_k^l].$$

We derive diagonal and off-diagonal entries in $\text{Cov}[u_{l+1}(\tilde{h}_k^l)]$ separately. We obtain for $i = j$

$$\begin{aligned} \text{Cov}(u_{l+1}(\tilde{h}_k^l)_i, u_{l+1}(\tilde{h}_k^l)_i) &= \mathbb{E} \left[(u_{l+1}(\tilde{h}_k^l)_i)^2 \right] - \mathbb{E}[u_{l+1}(\tilde{h}_k^l)_i]^2 \\ &= \mathbb{E} \left[(\tilde{h}_{k_i}^l)^2 \right] \mathbb{E}[(\beta_{k_i}^l)^2] - q^2 \mathbb{E}[\tilde{h}_{k_i}^l]^2 \\ &= q \mathbb{E} \left[(\tilde{h}_{k_i}^l)^2 \right] - q^2 \mathbb{E}[\tilde{h}_{k_i}^l]^2 \\ &= q \text{Cov}(\tilde{h}_{k_i}^l, \tilde{h}_{k_i}^l) + q \mathbb{E}[\tilde{h}_{k_i}^l]^2 - q^2 \mathbb{E}[\tilde{h}_{k_i}^l]^2 \\ &= q \text{Cov}(\tilde{h}_{k_i}^l, \tilde{h}_{k_{k_i}}^l) + q(1 - q) \mathbb{E}[\tilde{h}_{k_i}^l]^2 \end{aligned}$$

and for $i \neq j$

$$\begin{aligned} \text{Cov}(u_{l+1}(\tilde{h}_k^l)_i, u_{l+1}(\tilde{h}_k^l)_j) &= \mathbb{E} \left[u_{l+1}(\tilde{h}_k^l)_i u_{l+1}(\tilde{h}_k^l)_j \right] - \mathbb{E}[u_{l+1}(\tilde{h}_k^l)_i] \mathbb{E}[u_{l+1}(\tilde{h}_k^l)_j] \\ &= \mathbb{E} \left[\tilde{h}_{k_i}^l \tilde{h}_{k_j}^l \beta_{k_i}^l \beta_{k_j}^l \right] - q^2 \mathbb{E}[\tilde{h}_{k_i}^l] \mathbb{E}[\tilde{h}_{k_j}^l] \\ &= q^2 \mathbb{E} \left[\tilde{h}_{k_i}^l \tilde{h}_{k_j}^l \right] - q^2 \mathbb{E}[\tilde{h}_{k_i}^l] \mathbb{E}[\tilde{h}_{k_j}^l] \\ &= q^2 \text{Cov}(\tilde{h}_{k_i}^l, \tilde{h}_{k_j}^l). \end{aligned}$$

By vectorizing and rescaling with q we obtain the final expression.

The Jacobian of the dropout layer is the identity matrix:

$$\mathbb{E} \left[\nabla_{\tilde{h}_k^l} g_{l+1}(\tilde{h}_k^l) \right] = \mathbb{E} [I z_k^l / q] = I. \quad (33)$$

D Algorithm

Below we present our proposed algorithm BMM. For notational simplicity we consider the equally spaced time series $Y = \{y(t_1), \dots, y(t_N)\}$ with step size Δt and a discretization with the same step size, such that $y(t_n) = y_k$. The discretization can be chosen arbitrarily and dynamically if desired. Our method can be used for deterministic evaluation of the data fit term in the ELBO training objective or deterministic predictions during test.

Algorithm 1 Bidimensional Moment Matching (BMM)

Inputs: $f_\theta(\cdot) := u_L(u_{L-1}(\dots u_2(u_1(\cdot)) \dots))$ ▷ NSDE, drift net
 $L_\phi(\cdot) := v_L(v_{L-1}(\dots v_2(v_1(\cdot)) \dots))$ ▷ NSDE, diffusion net
 $q(z(t_0))$ ▷ Recognition Model
 $p(y(t_n)|z(t_n))$ ▷ Likelihood function
 $Y = \{y(t_1), \dots, y(t_N)\}$ ▷ Time series

Outputs (Training): $\mathbb{E}_{q(Z)} [\log p(Y|Z)]$
Outputs (Prediction): $\mathbb{E}_{q(Z)} [p(Y|Z)]$

$\mu_0, \Sigma_0 \leftarrow q(z_0)$ ▷ Marginal at initial time point
for time step $k \in \{0, \dots, K-1\}$ **do** ▷ Horizontal Moment Matching, K can be chosen freely for prediction
 $\tilde{h}_k^0, \tilde{e}_k^0 \leftarrow \mathcal{N}(\mu_k, \Sigma_k)$ ▷ Input distribution to drift and diffusion net
for layer index $l \in \{1, \dots, L\}$ **do** ▷ Vertical Moment Matching along NSDE layers
See Appx. C for expectation, covariance, and Jacobian of u_l and v_l
 $a_k^l \leftarrow \mathbb{E}[u_l(\tilde{h}_k^{l-1})]$ ▷ Drift net, expectation at layer l
 $B_k^l \leftarrow \text{Cov}[u_l(\tilde{h}_k^{l-1})]$ ▷ Drift net, covariance at layer l
 $\tilde{h}_k^l \leftarrow \mathcal{N}(a_k^l, B_k^l)$ ▷ Drift net, output distribution at layer l
 $J_k^l \leftarrow \mathbb{E}[\nabla_{\tilde{h}_k^{l-1}} u_l(\tilde{h}_k^{l-1})]$ ▷ Drift net, Jacobian at layer l
 $c_k^l \leftarrow \mathbb{E}[v_l(\tilde{e}_k^{l-1})]$ ▷ Diffusion net, expectation at layer l
 $D_k^l \leftarrow \text{Cov}[v_l(\tilde{e}_k^{l-1})]$ ▷ Diffusion net, covariance at layer l
 $\tilde{e}_k^l \leftarrow \mathcal{N}(c_k^l, D_k^l)$ ▷ Diffusion net, output distribution at layer l
end for
 $D_k \leftarrow (D_k^L + (c_k^L)(c_k^L)^T) \odot I$ ▷ Diffusion net, second central moment
 $C_k \leftarrow \Sigma_k \prod_{l=1}^L J_k^l$ ▷ Stein's lemma
 $\mu_{k+1} \leftarrow \mu_k + a_k^L \Delta t$ ▷ Mean at time step $k+1$
 $\Sigma_{k+1} \leftarrow \Sigma_k + B_k^L \Delta t^2 + (C_k + C_k^T) \Delta t + D_k \Delta t$ ▷ Covariance at time step $k+1$
end for
Depending on $p(y(t_n)|z(t_n))$ the below integrals are analytically available or require numerical approximation (e.g. VMM)
Training:
for time step $k \in \{1, \dots, K\}$ **do**
 $\mathbb{E}_{q(z_k)} [\log p(y_k|z_k)] \leftarrow \int \log p(y_k|z_k) \mathcal{N}(z_k|\mu_k, \Sigma_k) dz_k$ ▷ Marginal log likelihood at step k
end for
return $\mathbb{E}_{q(Z)} [\log p(Y|Z)] = \sum_{k=1}^K \mathbb{E}_{q(z_k)} [\log p(y_k|z_k)]$
Prediction:
for time step $k \in \{1, \dots, K\}$ **do**
 $\mathbb{E}_{q(z_k)} [p(y_k|z_k)] \leftarrow \int p(y_k|z_k) \mathcal{N}(z_k|\mu_k, \Sigma_k) dz_k$ ▷ Marginal likelihood at step k
end for
return $\mathbb{E}_{q(Z)} [p(Y|Z)] = \mathbb{E}_{q(z_K)} [\dots \mathbb{E}_{q(z_1)} [p(y_1|z_1)] \dots]$

E Cubature

Cubature is a well known numerical integration method, which estimates the expected value of a nonlinear function $f(z_k)$ with respect to a Gaussian density $\mathcal{N}(z_k|\mu_k, \Sigma_k)$ as a weighted sum of point mass evaluations

$$\int f(z_k) \mathcal{N}(z_k|\mu_k, \Sigma_k) dz_k \approx \sum_{i=1}^C w_i f(\mu_k + \sqrt{\Sigma_k} \zeta_i), \quad (34)$$

where $\sqrt{\Sigma_k} \sqrt{\Sigma_k}^T = \Sigma_k$. The coefficients w_i and ζ_i are predetermined by a heuristic that aims to spread the particles around the support of the distribution in a maximally information preserving way. There exist multiple heuristics for choosing w_i and ζ_i . Such a heuristic is the *Unscented Transform* (UT), which is commonly used in the context of Kalman filtering [Wan & Merwe \[2000\]](#). UT can be formulated as a sum of $2D+1$ elements for a D -dimensional input space as

$$w_i = \begin{cases} \frac{\lambda}{D+\kappa} & , i = 0, \\ \frac{1}{2(D+\kappa)} & , i = 1, \dots, 2D, \end{cases} \quad (35)$$

$$\zeta_i = \begin{cases} 0 & , i = 0, \\ \sqrt{\lambda + D}e_i & , i = 1, \dots, D, \\ -\sqrt{\lambda + D}e_{i-D} & , i = D + 1, \dots, 2D. \end{cases} \quad (36)$$

The constants λ and κ control the particle spread. The vectors e_i form the standard basis in D dimensions.

F Experimental Details

Both drift and diffusion neural nets are trained for the NSDE variants by minimizing the ELBO, as proposed in Eq. 6. We use the Adam optimizer [Kingma & Ba \[2015\]](#) and its default hyperparameter settings. Number of epochs and other method specific hyperparameters have been tuned manually for each method. We use a RK4 discretization for NODE and backpropagate directly through the solver.

Experiments have been performed using PyTorch [\[Paszke et al., 2017\]](#), which is available under the BSD license.

Lotka-Volterra. We choose stochastic Lotka-Volterra equations as in [Abbati et al. \[2019\]](#)

$$dx_t = \begin{bmatrix} 2x_{t,1} - x_{t,1}x_{t,2} \\ x_{t,1}x_{t,2} - 4x_{t,2} \end{bmatrix} dt + \sqrt{\begin{bmatrix} 0.05 & 0.03 \\ 0.03 & 0.09 \end{bmatrix}} dw_t.$$

We generate 128 paths using Euler-Maruyama discretization with a small step size of $dt = 10^{-5}$ seconds. Afterwards, we coarsen the data set such that 200 equally spaced observations between 0–10 seconds remain. First 100 observations are used for training and the remaining 100 observations for testing. We use a batch size of 16 and a prediction horizon of $s = 10$ for training. Experiments have been run on a CPU Intel i5.

Beijing Air Quality. The atmospheric air-quality data set from Beijing [\[Zhang et al., 2017\]](#) consists of hourly measures over the period 2014-2016 at three different locations. The air quality is characterized by 10 different features at each location. Including the timestamp we obtain in total 34 features. We follow [Jorgensen et al. \[2020\]](#) for designing the experimental setup. The first two years of are used for training and we test on the first 48 hours in the year 2016. We use a batch size of 16 and a prediction horizon of $s = 10$ for training. Experiments have been run on a CPU Intel Xeon. The dataset is available [here](#). It is unknown to us under which license the data set is published. We contacted the authors of the data set and received their permission to use this data set in this publication.

3-DOF-Robot. The 3-DOF-Robot dataset [\[Agudelo-España et al., 2020\]](#) consists of multiple trajectories with length 14000, 3 input and 9 output dimensions, recorded with a sampling rate of 1kHz. The dataset was recorded at two different operating modes: (i) 50 recordings of low frequency oscillations of the robot arm with a small moving range, and (ii) 50 recordings of high frequency oscillations with full moving range. We train on the first 38 trajectories and validate on the next 3 trajectories using the low frequency recordings. Test is performed on last 9 low frequency trajectories, denoted as IID, and last 9 high frequency recordings, denotes as Transfer. We use a batch size of 16 and a prediction horizon of $s = 16$ for training. Experiments have been run on a CPU Intel Xeon. The dataset is available [here](#) under the MIT license.

G Expectation of Coverage Probability Error

The prediction quality is assessed in terms of *mean squared error* (MSE), *negative log-likelihood* (NLL), as well as the *expectation of coverage probability error* (ECPE). ECPE measures the absolute difference between true confidence and the empirical coverage probability as [\[Cui et al., 2020\]](#)

$$ECPE = \frac{1}{n} \sum_{n=1}^N |\hat{p}_j - p_j|, \quad (37)$$

where p_j and \hat{p}_j is the true frequency and empirical frequency, respectively. We choose 11 equally spaced confidence levels between 0 and 1. By taking the average over all test samples $x_k \in \mathcal{D}_{test}$, which lie in a predicted confidence interval, the empirical frequency is estimated as

$$\hat{p}_j = \frac{\sum_k^{|\mathcal{D}_{test}|} \mathbb{I}\{x_k \leq \hat{F}_k^{-1}(p_j)\}}{|\mathcal{D}_{test}|}. \quad (38)$$

In contrast to Cui et al. [2020], we consider in our work the case of multivariate predictors, which complicates the estimation of the predicted inverse cumulative distribution function \hat{F}_k^{-1} . However, if x_k is normally distributed, we can analytically estimate \hat{F}_k^{-1} as a function of model outputs μ_k and Σ_k . As discussed by Bensimhou [2013], we may define the cumulative distribution function as the probability that a sample lies inside the ellipsoid determined by its Mahalanobis distance r . The ellipsoidal region is analytically obtained as

$$(x_k - \mu_k)^T \Sigma_k^{-1} (x_k - \mu_k) \leq \chi_D^2(p) = \hat{F}_k^{-1}(p), \quad (39)$$

where χ_D^2 is the chi-squared distribution with D degrees of freedom.

H Network Architecture

For all experiments we use similar architectures as competing methods. For NSDEs with cubature we use the same architectures except exchanging ReLU with tanh. We assume in all experiments that $p(y_k|z_k) = N(y_k|z_k, cI)$ for a fixed $c > 0$, $q(z_0) = N(z_0|\mu_0, \Sigma_0)$, and $p(z_0) = N(z_0|0, I)$.

Lotka-Volterra.

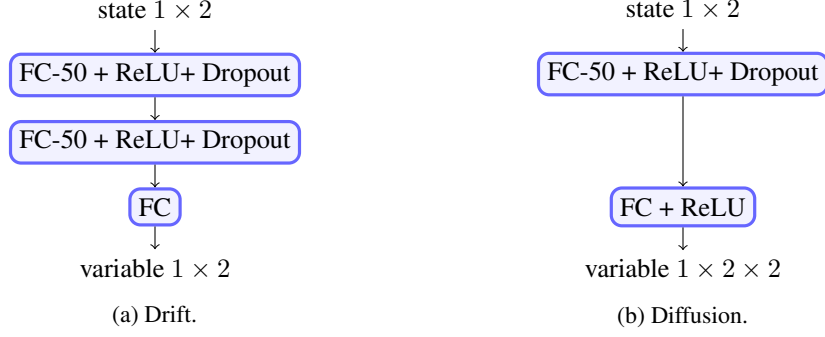


Figure 7: NSDE architecture for Lotka-Volterra experiment.

Beijing Air Quality.

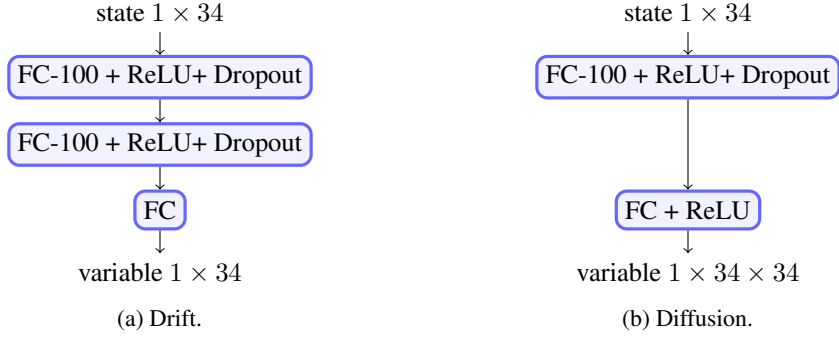


Figure 8: NSDE architecture for Air quality experiment.

3-DOF-Robot.

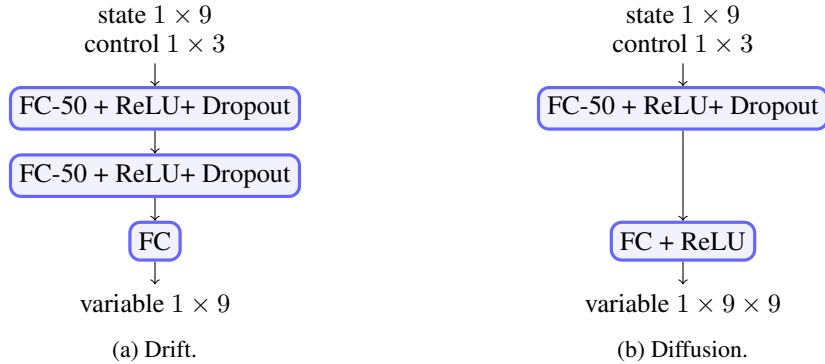


Figure 9: NSDE architecture for 3-DOF-Robot experiment.